

Spin-Orbit Resonance and the Evolution of Compact Binary Systems

Jeremy D. Schnittman

Department of Physics, MIT, 77 Massachusetts Ave., Cambridge, MA 02139

Starting with a post-Newtonian description of compact binary systems, we derive a set of equations that describes the evolution of the orbital angular momentum and both spin vectors during inspiral. We find regions of phase space that exhibit resonance behavior, characterized by small librations of the spin vectors around a fixed orientation. Due to the loss of energy and orbital angular momentum through radiation reaction, systems can eventually be captured into these resonance orientations. By investigating the long-term evolution of compact binaries with a variety of initial conditions, we find that the distribution in parameter space can be strongly affected by resonance captures. This has the effect of significantly reducing the size of search space for gravitational wave sources, in turn improving the chances of detecting such sources through methods of template matching. Furthermore, by calculating the expected spin distribution at the end of the inspiral phase, we can predict what are the most likely initial conditions for the plunge phase, a result of great interest for numerical relativity calculations.

PACS numbers: 04.25.Nx, 04.30.Db, 95.30.Sf

I. INTRODUCTION

The inspiral and subsequent coalescence of two black holes (BH) or neutron stars (NS) promises to be a strong source of gravitational waves for a number of new interferometric detectors currently being developed¹. In order to successfully detect and then analyze such sources, we need to have an accurate description of the gravitational waveforms they will produce. For longer signals lasting many orbital cycles (typically NSs in the LIGO frequency band and BHs in the LISA band), the detection methods rely heavily on a technique called matched filtering. This method is based on the premise that we can calculate theoretical templates of gravitational waves which in turn are cross-correlated with the observed data in an attempt to match a small amplitude signal buried under high background noise. Since the anticipated signal can be hundreds or even thousands of cycles long, it is critical that the form of the theoretical template is very accurate or the detection could be missed. Once detected, the observed waveform must then be compared to a larger collection of model templates in order to fit the binary parameters and determine their statistical confidences.

Approximate templates that do not include spin effects have been shown to have a poor chance of matching gravitational waveforms from spinning binaries [1, 2, 3, 4, 5, 6]. Even if we were able to calculate the theoretical waveforms with perfect physical accuracy, the binary black hole system is so complicated that we would need a very large template library to give a reasonable chance at detection [3, 7]. For two spinning black holes, the parameter space is characterized by at least 11 intrinsic variables [the masses (2), the angular momentum vector (3), and two spin vectors (6)]. Apostolatos et al. [8] showed that the two-spin system can be reduced in the limits of equal mass when neglecting spin-spin interactions and later Apostolatos [9] included these terms for the equal mass, equal spin case. Recent work by Buonanno et al. [7] showed that the size of this parameter space can also be reduced by considering a set of *quasi-physical* templates that mimic the physical behavior of two spins with a single effective spin. Grandclement et al. [5] have suggested a different method of using “spiked” templates to expand the search templates and simulate spin effects. While these fitting methods greatly aid the searches for gravitational waves, they could also benefit from additional astrophysical information about the systems that are producing the waves, as well as their evolution up to the point where they enter the frequency regime of the detector. The added advantage of using strictly physical templates is the direct manner in which they allow us to determine the intrinsic parameters of the compact binary.

There are a number of stellar evolution models that describe the formation of binary black hole systems, including estimates for initial spins and kick velocities, which in turn can give the orientation of the orbit [10, 11, 12, 13]. However, there is still a fair amount of uncertainty in the appropriate initial values to use for inspiraling stellar mass

¹ <http://www.ligo.caltech.edu/>
<http://www.virgo.infn.it>
<http://www.geo600.uni-hannover.de>
<http://tamago.mtk.nao.ac.jp>
<http://lisa.nasa.gov>

black hole binaries. The mechanisms governing supermassive or intermediate mass black hole mergers are even less certain. In both cases, we have little or no idea what to expect the system might look like as it enters the final stages of evolution towards inspiral and merger.

In addition to the compact objects formed through binary stellar evolution, another important source of gravitational waves may be capture binaries [14]. These include binary systems that form in the cores of dense globular clusters, stellar mass and supermassive black holes in the centers of galaxies, and supermassive black hole binaries formed through hierarchical galactic mergers. Many of these systems should have no a priori preference for any particular spin orientation. It is also possible that some of these systems have already been seen, but not through the detection of gravitational waves. A recently discovered binary pulsar system may give important information about the initial spin-orbit orientations and early evolution of inspiraling neutron stars [15, 16]. Merritt & Ekers [17] suggest that the morphology of radio jets from active galaxies may point to recent supermassive BH mergers and resulting changes in spin orientation. In fact, the longer term merger history of a supermassive black hole might also be inferred by its current mass and spin [18]. If we could give a realistic prediction of the orientation of both spins and the angular momentum vector relative to each other at the time of inspiral, an important link between these different branches of astrophysics could be established. A successful identification with an electromagnetic source would also be critical in the confirmation of any gravitational wave detection, especially in the early years of gravitational wave astronomy.

To further investigate these issues, we have developed a code to integrate the post-Newtonian equations of motion and spin precession for two spinning point masses including radiation reaction. The full evolution of the system from its formation until merger covers an enormous range of time scales, from hundreds of megayears to fractions of milliseconds. To accommodate this range, we first derive an orbit-averaged system of evolution equations that model the orientation of the spins and angular momentum without actually following the orbital phase of the binary. These orbit-averaged equations of motion agree quite well with the full 2.5-order post-Newtonian equations for modeling the evolution of the orbital angular momentum and both spin vectors [19].

With this orbit-averaged formulation, a collection of equilibrium solutions are found in which the relative orientation of the spin vectors and orbital angular momentum remains fixed in time. Furthermore, we find that the majority of these equilibrium solutions are stable, so systems nearby in parameter space librate around the stable orbits like a spin-orbit or spin-spin resonance. With the inclusion of radiation reaction, spin-locked systems remain locked, following a trajectory along equilibrium solutions with steadily decreasing orbital angular momentum. Furthermore, initially non-resonant systems can actually be captured into these stable orbits and then oscillate around a fixed orientation throughout the rest of the inspiral process.

One effect of this resonance behavior is to significantly reduce the size of the parameter space over which the spin orientations are distributed. In turn, this could have an important impact on the size of the template library used for waveform matching. Instead of including a separate template for every single spin orientation (at least four parameters), we could instead use a one- or two-dimensional family of equilibrium solutions as representative of the entire sample. These “guiding center” waveforms would be a good match for any resonant system, librating around the equilibrium orientations, potentially reducing the size of the search space by orders of magnitude while maintaining a set of strictly physical templates.

Alternatively, we can take the inverse approach so that, given the gravitational wave form of an inspiraling binary, we should be able to infer the evolutionary history leading up to the point where it enters the detector frequency band. In this manner, perturbative methods could be used to explore the phase space around the equilibrium regions and better pinpoint the exact binary parameters of the detected signal. Eventually, as the detection rate increases to hundreds or even thousands of signals per year, we will be able to fully map out the spin distribution of compact binaries in the Universe and thus test the theoretical results presented in this paper.

In addition to reducing the volume of parameter space in the template library, the equilibrium solutions could be extremely important for determining initial conditions for the plunge calculations. This phase of the binary merger is widely regarded as the least-well understood physically and at the present time we have relatively little faith in any theoretical waveforms that might describe the plunge (see, e. g. [20] and references therein). Since the post-Newtonian expansion (known at this point up to terms of order 3.5PN) becomes less and less accurate in the plunging region, it is likely that we will need to rely on full numerical relativity calculations to produce the transitional waveforms linking the long inspiral and the ring-down phase (which is itself well described by perturbative methods). Because of the prohibitive computational expense of these calculations, it is that much more important to have a solid understanding of how to describe the initial conditions. We believe that the equilibrium solutions described in this paper are an excellent place to begin, as they may represent a large segment of the relevant binary population. Knowing the final spin orientation at the plunge phase would also improve our understanding of black hole recoil velocities, a field of much recent interest [21].

In Section II we present the evolution equations and discuss the relevant time scales for the binary inspiral and spin precession. In Section III we show how this system of equations can be further reduced to five variables (four when assuming circular orbits), which completely describe the relative orientation of the compact objects, and how

this reduced system exhibits resonance behavior. Section IV describes the evolution of such a system under radiation reaction and the dependence on initial conditions. In Sections V and VI we discuss the effects of large mass ratios, eccentric orbits, and the dependence on spin magnitude. We conclude with a discussion of the astrophysical implications of these results and directions for future work.

II. BINARY EVOLUTION EQUATIONS

We use the post-Newtonian equations of motion for the reduced two-body problem including Lense-Thirring precession terms for the point mass spins. Throughout this paper we adopt geometrized units with $G = c = 1$. The instantaneous precession equations are (see, e. g. [8, 19, 22])

$$\dot{\mathbf{S}}_1 = \boldsymbol{\Omega}_1 \times \mathbf{S}_1 \quad (2.1a)$$

$$\dot{\mathbf{S}}_2 = \boldsymbol{\Omega}_2 \times \mathbf{S}_2, \quad (2.1b)$$

where

$$\boldsymbol{\Omega}_1 = \frac{1}{r^3} \left[\left(2 + \frac{3m_2}{2m_1} \right) \mathbf{L}_N - \mathbf{S}_2 + 3(\hat{\mathbf{r}} \cdot \mathbf{S}_2)\hat{\mathbf{r}} \right] \quad (2.2a)$$

$$\boldsymbol{\Omega}_2 = \frac{1}{r^3} \left[\left(2 + \frac{3m_1}{2m_2} \right) \mathbf{L}_N - \mathbf{S}_1 + 3(\hat{\mathbf{r}} \cdot \mathbf{S}_1)\hat{\mathbf{r}} \right]. \quad (2.2b)$$

Here $\mathbf{S}_{1,2}$ are the spin vectors of the two compact objects with units of angular momentum and a dot represents time derivative (assuming a global coordinate time t in the post-Newtonian approximation). The bodies have masses $m_1 \geq m_2$ and are separated by a distance r in the $\hat{\mathbf{r}}$ direction. The Newtonian orbital angular momentum \mathbf{L}_N is defined in the usual way: $\mathbf{L}_N = \mu(\mathbf{r} \times \dot{\mathbf{r}})$ with the reduced mass defined as

$$\mu = \frac{m_1 m_2}{m} \quad (2.3)$$

and the total mass is $m = m_1 + m_2$.

At first glance, the leading r^{-3} terms in equations (2.2a,2.2b) suggest that spin precession only becomes important late in the inspiral when r becomes small. However, since the great majority of the evolution (in terms of time) occurs at a large separation, the spins actually have a chance to undergo a large number of slow precessions leading up to the inspiral phase. To first order, the evolution of a circular orbit due to gravitational radiation is [23]

$$r(t) = (r^4(0) - \alpha t)^{1/4}, \quad (2.4)$$

where $\alpha = \frac{256}{5}\mu m^2$, giving

$$\frac{dr}{dt} = -\frac{\alpha}{4}(r^4(0) - \alpha t)^{-3/4}. \quad (2.5)$$

We can thus define a characteristic time scale for inspiral as

$$T_{\text{inspiral}} \equiv \frac{r}{dr/dt} \sim r^4. \quad (2.6)$$

The precession time scale is given to leading order as

$$T_{\text{prec}} \equiv |\Omega|^{-1} \sim \frac{r^3}{L_N} \sim r^{5/2}. \quad (2.7)$$

For large r , the precession time scale is actually shorter than the inspiral time scale, and thus we see that the spin-orbit effects are important even at early times.

At these large separations, the system evolves very slowly in time, with an orbital period much shorter than the precession period. The number of orbits N_{orb} at a given separation r and orbital period T_{orb} is given by

$$\frac{dN_{\text{orb}}}{dr} = \frac{1}{T_{\text{orb}}} \left(\frac{dr}{dt} \right)^{-1} \sim r^{3/2} \quad (2.8)$$

while the number of precession cycles N_{prec} is given by

$$\frac{dN_{\text{prec}}}{dr} = \frac{1}{T_{\text{prec}}} \left(\frac{dr}{dt} \right)^{-1} \sim r^{1/2}. \quad (2.9)$$

In short, this means we must calculate the spin evolution over a large range of r , corresponding to a very large number of orbits. However, since we are interested here in the net evolution of the spin orientation, the actual phase of the binary orbit can be ignored and equations (2.2a) and (2.2b) can be calculated in an orbit-averaged approximation (see Appendix A). Generalizing to non-circular orbits with semimajor axis a and eccentricity e , the orbit-averaged precession vectors are

$$\bar{\boldsymbol{\Omega}}_1 = \frac{1}{a^3(1-e^2)^{3/2}} \left[\left(2 + \frac{3m_2}{2m_1} - \frac{3\mathbf{S}_2 \cdot \mathbf{L}_N}{L_N^2} \right) \mathbf{L}_N + \frac{1}{2} \mathbf{S}_2 \right] \quad (2.10a)$$

and

$$\bar{\boldsymbol{\Omega}}_2 = \frac{1}{a^3(1-e^2)^{3/2}} \left[\left(2 + \frac{3m_1}{2m_2} - \frac{3\mathbf{S}_1 \cdot \mathbf{L}_N}{L_N^2} \right) \mathbf{L}_N + \frac{1}{2} \mathbf{S}_1 \right]. \quad (2.10b)$$

An interesting result is that the orbit-averaged precession equations are independent of the ellipse's orientation in the plane normal to \mathbf{L}_N . In other words, the first-order post-Newtonian (1PN) effect of pericenter precession does not play a role in the spin evolution, which is fortunate because of the relatively short time scales involved, compared to the slower effects of spin-orbit acceleration (1.5PN), spin-spin acceleration (2PN), and radiation reaction (2.5PN) [19, 22]. In the orbit-averaged equations of motion, the spin-orbit precession terms (1PN) dominate on a short time scale, but the secular effects of the radiation reaction are also very important in the long-term evolution of the system.

On time scales short compared to the inspiral time, the total angular momentum

$$\mathbf{J} = \mathbf{L}_N + \mathbf{S} = \mathbf{L}_N + \mathbf{S}_1 + \mathbf{S}_2 \quad (2.11)$$

is conserved, implying that the orbital angular momentum evolves according to

$$\dot{\mathbf{L}}_N = -\dot{\mathbf{S}} \sim \frac{1}{r^3} \mathbf{S}_{\text{eff}} \times \mathbf{L}_N, \quad (2.12)$$

where \mathbf{S}_{eff} is some linear combination of \mathbf{S}_1 and \mathbf{S}_2 (note this is *not* the same effective spin as in [7]). Since $\mathbf{L}_N \cdot \dot{\mathbf{L}}_N = 0$, without radiation reaction, the magnitude of the orbital angular momentum vector is constant with spin precession. The magnitude of the total spin vector \mathbf{S} , on the other hand, is *not* conserved as the angle changes between the two spin vectors (each of constant magnitude).

The relations (2.11) and (2.12) constrain the binary system to a subset of the complete parameter space defined by the three vectors \mathbf{L}_N , \mathbf{S}_1 , and \mathbf{S}_2 . We believe it is this set of constraints that best explains much of the behavior presented below, as opposed to a more classical description of resonance based on Hamiltonian mechanics and energy minima in phase space (see, e. g. Murray & Dermott [24], Sussman & Wisdom [25]). However, a Hamiltonian formulation of the post-Newtonian equations of motion such as in [26, 27, 28] may prove to give a more classical explanation to these apparently geometric constraints.

The inclusion of gravitational radiation causes the orbit to shrink and also circularize in time, reducing a , e , and the magnitude of the angular momentum

$$L_N = \mu \sqrt{ma(1-e^2)}. \quad (2.13)$$

Following Peters [23] and adopting units with $m = 1$, we use the coupled first order differential equations

$$\frac{d}{dt} a = -\frac{64}{5} \frac{\mu}{a^3(1-e^2)^{7/2}} \left(1 + \frac{73}{24} e^2 + \frac{37}{96} e^4 \right), \quad (2.14)$$

$$\frac{d}{dt}e = -\frac{304}{15} \frac{\mu e}{a^4(1-e^2)^{5/2}} \left(1 + \frac{121}{304}e^2\right), \quad (2.15)$$

and

$$\frac{d}{dt}\mathbf{L}_N = -\frac{32}{5} \frac{\mu^2}{a^{7/2}(1-e^2)^2} \left(1 + \frac{7}{8}e^2\right) \hat{\mathbf{L}}_N \quad (2.16)$$

to evolve the binary orbital elements in time. All of the above orbit-averaged precession and radiation reaction equations have been tested and compared to the full 2.5-order post-Newtonian equations of motion in Kidder [19]. The agreement is very good for most of the inspiral, all the way down to $r \lesssim 10m$, after which almost any post-Newtonian approximation becomes increasingly uncertain.

III. GEOMETRY OF EQUILIBRIUM

One of the most difficult aspects of studying the spinning binary system is the problem of visualizing and analyzing the orientation of the two spins and the angular momentum in an informative way. In general, these three vectors are defined by nine coordinates [the angular momentum is also related to a and e through (2.13)]. Since the spin magnitudes S_1 and S_2 are conserved in the point mass approximation, and we can pick a coordinate system where \mathbf{L}_N points in the $\hat{\mathbf{e}}_z$ direction, we are left with five coordinates: $(L_N, \theta_1, \theta_2, \phi_1, \phi_2)$. Furthermore, the overall dynamics are preserved under rotation around \mathbf{L}_N so we can reduce the spin degrees of freedom by defining the $\hat{\mathbf{e}}_x$ direction along $\phi_1 = 0$, leaving four independent coordinates to define the orientation of the system: $(L_N, \theta_1, \theta_2, \Delta\phi)$. Figure 1 shows a schematic of the geometry used throughout this paper. Following the post-Newtonian formalism, all angles and vector magnitudes are defined in a Cartesian, flat space-time.

In this coordinate system, there exists a set of equilibrium spin configurations for which L_N, θ_1, θ_2 , and $\Delta\phi$ are constant (without radiation reaction), even though the individual vectors might vary in time from the point of view of a fixed inertial coordinate system. Trivial equilibrium examples include the collinear cases with $\cos\theta_1 = \pm 1$ and $\cos\theta_2 = \pm 1$. More interesting cases occur when $\mathbf{S}_1, \mathbf{S}_2$, and \mathbf{L}_N all appear to precess around a fixed axis at a constant rate so as to remain in a fixed relative orientation. These points in parameter space can be found by solving (cf. Apostolatos [9])

$$\frac{d}{dt}(\mathbf{S}_1 \cdot \mathbf{S}_2) = \frac{3}{2a^3(1-e^2)^{3/2}} \left[\frac{m_2}{m_1} - \frac{m_1}{m_2} + \frac{(\mathbf{S}_1 - \mathbf{S}_2) \cdot \mathbf{L}_N}{L_N^2} \right] \mathbf{S}_2 \cdot (\mathbf{L}_N \times \mathbf{S}_1) = 0. \quad (3.1)$$

Note that the last term (a vector triple-product) can be written in our reduced coordinate system as

$$\mathbf{S}_2 \cdot (\mathbf{L}_N \times \mathbf{S}_1) = S_1 S_2 L_N \sin\theta_1 \sin\theta_2 \sin\Delta\phi. \quad (3.2)$$

Thus (3.1) is satisfied when $\mathbf{S}_1, \mathbf{S}_2$, and \mathbf{L}_N are coplanar, i.e. $\sin\Delta\phi = 0$ for all times. In practice this means finding simultaneous solutions to

$$\mathbf{S}_2 \cdot (\mathbf{L}_N \times \mathbf{S}_1) = 0 \quad (3.3)$$

and

$$\frac{d}{dt}[\mathbf{S}_2 \cdot (\mathbf{L}_N \times \mathbf{S}_1)] = 0. \quad (3.4)$$

Combining with equations (2.2a, 2.2b, 2.10a, and 2.10b), (3.4) can be written in terms of just $\mathbf{S}_1, \mathbf{S}_2$, and \mathbf{L}_N , with no explicit time derivatives:

$$(\boldsymbol{\Omega}_1 \times \mathbf{S}_1) \cdot [\mathbf{S}_2 \times (\mathbf{L}_N + \mathbf{S}_1)] = (\boldsymbol{\Omega}_2 \times \mathbf{S}_2) \cdot [\mathbf{S}_1 \times (\mathbf{L}_N + \mathbf{S}_2)], \quad (3.5)$$

which in turn are simple combinations of our reduced coordinates $(L_N, \theta_1, \theta_2, \Delta\phi)$.

For a given value of L_N (i. e. at a particular point in time during the binary inspiral), and setting $\sin\Delta\phi = 0$, solutions of (3.5) trace out one-dimensional curves in (θ_1, θ_2) space. Figure 2 shows these curves for two maximally spinning black holes with nearly equal masses ($m_1 = 0.55, m_2 = 0.45$) at a few stages of the inspiral evolution ($L_N = 4, 3, 2, 1, 0.5$, with binary separations of $r/m \approx 260, 150, 65, 16, 4$). These solutions correspond to the aligned

configuration with $\Delta\phi = 0$ and are found numerically to be stable, as will be explained below. There also exist anti-aligned equilibrium curves for $\Delta\phi = 180^\circ$, shown in Figure 3 for the same masses and values of L_N . We find that the curves along the bottom ($\theta_2 \lesssim 50^\circ$) and the right side ($\theta_1 \gtrsim 140^\circ$) of the plot correspond to stable equilibria, while the solutions in the upper left corner, appearing at later times, are generally unstable or quasi-stable.

The regions of stability can be better understood by considering a type of effective potential for orbits in parameter space near the equilibrium solutions. While the precession equations do not suggest any obvious way of being reformulated in the traditional approach of an analytic effective potential, we can map out the potential numerically by integrating a large sample of initial conditions. For each of these initial conditions, the stability of the spin orientation can be measured by integrating the change in $\Delta\phi$:

$$[\Delta\phi(t)]_{\text{tot}} = \int_{t_0}^t \frac{d}{dt'} \Delta\phi(t') dt'. \quad (3.6)$$

With this definition, $[\Delta\phi(t)]_{\text{tot}}$ is potentially unbounded and can grow in magnitude larger than 360° as one spin precesses around \mathbf{L}_N more rapidly and repeatedly “passes” the other spin vector. For binaries locked in a spin equilibrium (with either $\Delta\phi = 0^\circ$ or $\Delta\phi = 180^\circ$), the integrated phase shift will be zero. For systems far from this equilibrium, the two spins will precess more or less independently and will generally acquire a linear phase shift in time since $|\bar{\Omega}_1| \neq |\bar{\Omega}_2|$. And for systems *near* the equilibrium points in phase space, we expect the phase to librate around the exact coplanar solution given by equation (3.5).

Figure 4 shows $[\Delta\phi(t)]_{\text{tot}}$ for a few examples of these different regions in parameter space, again with $m_1 = 0.55$, $m_2 = 0.45$, and maximum spin parameters ($S_j = m_j^2$). Using Figures 2 and 3 as guides, we can identify initial conditions near stable and unstable equilibrium solutions. Figure 4a shows a binary near a stable equilibrium with $\theta_1 = 50^\circ$, $\theta_2 = 120^\circ$, $\Delta\phi = 0$, and $L_N = 4$. The system librates around $\Delta\phi = 0$ with amplitude of about 11° . For initial conditions far away from equilibrium points, the two spins precess at independent rates, giving a roughly linear drift in phase, as seen in Figure 4b, which has initial conditions $\theta_1 = 120^\circ$, $\theta_2 = 50^\circ$, $\Delta\phi = 0$, and $L_N = 4$. These two examples are also labeled on Figure 2 as ‘A’ and ‘B’.

For the systems oscillating around a stable equilibrium, we can think of an effective potential whose form can be inferred by the libration of trajectories through those points in phase space. With this approach, the minima of the potential lie along the solid curves plotted in Figures 2 and 3. Systems lying near these curves in parameter space will oscillate around them with constant amplitude and frequency. Phase space trajectories like the one in Figure 4b correspond to a plateau-type region of the effective potential with constant amplitude, where the spin vectors can precess freely through all values of $\Delta\phi$.

From this analysis, we can also determine that some of the equilibrium solutions plotted in Figure 3 are unstable (dashed lines). Perhaps it is more accurate to call these regions *quasi-stable* since initial conditions a small distance outside of these closed curves are found to exhibit behavior typical of trajectories near an unstable equilibrium: long periods of stasis followed by short bursts of rapid divergence away from equilibrium, as in Figure 4c ($\theta_1 = 30^\circ$, $\theta_2 = 133^\circ$, $\Delta\phi = 180^\circ$, $L_N = 1$, labeled ‘C’ on Figure 3). However, points just *inside* the equilibrium curves appear stable, librating around the locked $\Delta\phi = 180^\circ$ position in phase space.

In practice, we find that binaries initially outside of these quasi-stable regions tend to remain outside. Furthermore, when including radiation reaction, *all* binaries start outside of these regions, which only begin to appear for relatively small values of L_N late in the evolution. Thus it would be quite unlikely for an astrophysically realistic binary system to be found on the stable side of any of the quasi-stable equilibrium curves. Yet these regions are still of significant physical interest, as we believe the boundaries between stable and unstable regions in parameter space may be relevant to the ongoing question of chaos in spinning compact binaries and the existence of positive Lyapunov exponents in such systems (see, e. g. [29, 30]).

IV. SPIN EVOLUTION

In Section III, we assumed in the analysis that the orbital angular momentum L_N was constant in magnitude, i. e. there was no radiation reaction damping the system through gravitational wave emission. Of course, in all physically realistic black hole binaries, gravitational radiation will play a major role in the secular evolution of the orbit. From the post-Newtonian analysis in Section II, we see that both radiation reaction and spin precession are dynamically important through most of the long inspiral process.

With the inclusion of radiation reaction, the angular momentum evolves according to equations (2.12) and (2.16), changing direction due to Lense-Thirring precession and losing magnitude due to gravitational losses. The individual spin vectors still maintain constant magnitude under radiation reaction, but have access to a broader range of precession angles since the total angular momentum \mathbf{J} is no longer conserved. In this sense, radiation reaction removes an

integral of motion from the precession equations, allowing a greater region of phase space to be sampled throughout the inspiral evolution.

For the stable equilibrium solutions to equation (3.5), we find that the binary systems that lie on or sufficiently close to one of the curves in Figures 2 and 3 will evolve along successive curves of decreasing L_N as the system loses angular momentum to radiation reaction. At the same time, these stability regions grow stronger, confining a wider range of spins to the equilibrium curves. Even for some initial conditions that begin far away from the stable solutions, precessing freely through a large range of $\Delta\phi$, the effect of radiation reaction causes the spins to become locked and then librate around equilibrium. These systems undergo transitions from the “drifting” behavior of Figure 4b to the locked condition of 4a. Once the system becomes locked, we find it will stay locked throughout the rest of the inspiral.

The net effect of this spin evolution can be seen clearly in Figures 5 and 6. We show sinusoidal projections of the spin coordinates $(\theta_{12}, \Delta\phi)$ for an initially random, uniform distribution of spin vectors \mathbf{S}_2 . The polar angle θ_{12} is defined as the angle between the two spins: $\theta_{12} \equiv \cos^{-1}(\hat{\mathbf{S}}_1 \cdot \hat{\mathbf{S}}_2)$ and the azimuthal angle $\Delta\phi$ is defined as above. A sinusoidal projection maps a point with spherical coordinates (θ, ϕ) onto a plane with x-y coordinates given by $(\phi \sin \theta, \theta)$ so that equal areas in the plane correspond to equal solid angles on the sphere. This allows an accurate way of estimating the density of the distribution function in parameter space.

In Figure 5 we take a sample of initial conditions with $r/m = 1000$, $\theta_1 = 10^\circ$, and masses $m_1 = 0.55$, $m_2 = 0.45$. The relative spin orientation $(\theta_{12}, \Delta\phi)$ for the smaller black hole has a uniform random distribution, as shown in the upper-left frame of Figure 5. As the binaries evolve under radiation reaction, more of the initially unlocked spins become locked and then librate around $\Delta\phi = 0$, as seen in the second frame of Figure 5, corresponding to $r = 250m$. Once locked into an equilibrium spin orientation, the systems move along the curves shown in Figure 2, approaching the line $\theta_2 = \theta_1$ as $L_N \rightarrow 0$. This evolution is clearly evident in the last frame of Figure 5 as $\theta_{12}, \Delta\phi \rightarrow 0$ and the two spin vectors become closely aligned with each other (although not necessarily aligned with the orbital angular momentum). This result may have an important impact on the question of initial conditions for compact binaries entering the plunge and subsequent merger phase. While the general problem of two spinning black holes merging is still an open question in numerical relativity, it would certainly be a significant simplification if we can assume that the spins are initially aligned.

If we take the initial orientation of the more massive black hole spin to be retrograde with respect to the orbital angular momentum ($\theta_1 = 170^\circ$) and again evolve a uniform distribution of \mathbf{S}_2 orientations, we find a qualitatively different behavior. Instead of getting locked into the $\Delta\phi = 0$ equilibrium solutions of Figure 2 and evolving towards $\theta_{12} = 0$, the binaries approach the $\Delta\phi = 180^\circ$ solutions of Figure 3, where there is no strong correlation between θ_1 and θ_2 at late times. Thus as $L_N \rightarrow 0$ and $\Delta\phi \rightarrow 180^\circ$, the distribution in θ_{12} is roughly uniform, with a trend towards anti-alignment with $\theta_{12} > 90^\circ$. This is seen in the evolution of the spin distribution shown in Figure 6. Similar to Figure 5, a sample of spin orientations $(\theta_{12}, \Delta\phi)$ with uniform distribution is taken for the set of initial conditions with $r/m = 1000$ and $\theta_1 = 170^\circ$, plotted in a sinusoidal projection in the upper-left panel. As the systems evolve under radiation reaction, they approach an anti-aligned spin configuration with $\Delta\phi \rightarrow \pm 180^\circ$ and $\theta_{12} \approx 90^\circ - 180^\circ$.

We see from Figures 5 and 6 that the final spin configuration is strongly dependent on the initial orientation of the larger spin with respect to the orbital angular momentum. Figures 7 and 8 serve to quantify these effects for different initial values of θ_1 . When $\theta_1(t_0) \approx 0^\circ$, the final spins tend to be parallel, regardless of the initial orientation of \mathbf{S}_2 , as shown in Figure 7. However, if the smaller black hole initially has a retrograde orbit, the final spins tend towards the anti-aligned orientation described above (Figure 8). For the intermediate cases with $\theta_1(t_0) \approx 90^\circ$, there seems to be little net evolution in the relative spin distributions.

Given an initial probability distribution function $f(\theta_1)$, we can predict the final distribution of $(\theta_{12}, \Delta\phi)$ by weighting the ensemble of distributions in Figures 7 and 8 by $f(\theta_1)$. This initial spin distribution function has been the focus of much recent work in compact binary systems [10, 16]. Much of this work is based on the evolution of two large main-sequence stars that both eventually form compact objects through supernovae [31]. The resulting spin and angular momentum vectors are largely determined by the random kick given to each star during the asymmetric supernova explosions. Many of these kicks will disrupt the system entirely, while the undisrupted systems may end up with very different orientations than they had before the supernova. Using these binary evolution codes to give the initial angular momentum and spin orientations, we can then use the above results to evolve the compact binary system under radiation reaction into the detector frequency regime. According to Kalogera [10], a supernova kick velocity of $v_k \sim 200$ km/s should favorably produce a system with $\theta_1 < 30^\circ$. In this case, it follows that the $\Delta\phi = 0, \theta_{12} = 0$ equilibrium solution would well describe the orientation as the system enters the detector’s frequency range. However, even for systems locked in equilibrium, the *total* spin vector may not be parallel to the angular momentum vector, and thus simple precession Apostolatos et al. [8] of the orbital plane will still take place during the inspiral and must still be accounted for in the template libraries.

V. LARGE MASS RATIOS

Preliminary results with large mass ratios ($m_1 : m_2 > 1000$) show a similar behavior as the near-equal mass systems, although only for cases where $\theta_1(t_0)$ is close to zero [or alternatively $\theta_1(t_0) \approx 180^\circ$]. This might correspond to a supermassive black hole in the center of a galaxy surrounded by a large “accretion disk” of stellar-mass black holes and neutron stars [32]. If the smaller black holes begin with randomly oriented spins, then as they evolve towards merger, we find that θ_{12} remains roughly constant but $\Delta\phi \rightarrow 0$, as in the previous section. However, it is more likely that any massive stars formed in a self-gravitating accretion disk would *not* have random spin orientations, but rather be aligned with the angular momentum of the surrounding gas, and thus the central supermassive black hole, simplifying the problem even further.

If, on the other hand, the stellar-mass black holes originate from an isotropic population in the galactic bulge and sink towards the central black hole via dynamic friction, they should have initial velocities (i. e. orbital angular momentum) and spins with uncorrelated, uniform random distributions. In this case, the alignment effects described above are unlikely to be important, and the final spin and angular momentum orientations will likely have a similarly random distribution at the time of merger. While the large mass ratio limits the effect of spin locking, at the same time the spin ratio scales as m_2^2/m_1^2 , so to a large degree the smaller black hole can be treated as a point mass moving in a stationary spacetime, greatly reducing the parameter search space in any case [3].

For the moderate mass ratios ($m_1 : m_2 \approx 1 - 10$) for which resonance behavior *will* be important, one can estimate roughly the range over which the spin locking occurs during the binary inspiral by examining equation (3.1). To leading order, we can write the equilibrium condition as

$$\frac{d}{dt}(\cos \theta_{12}) \propto \left(\frac{m_2}{m_1} - \frac{m_1}{m_2} + \frac{S_1 \cos \theta_1 - S_2 \cos \theta_2}{L_N} \right) \approx 0. \quad (5.1)$$

Taking maximal spins and $L_N = \mu m^{1/2} r^{1/2}$, we can solve for the separation at which the resonance behavior begins to dominate the dynamics [maximizing r over the solution space to (5.1)]:

$$r_{\text{lock}}/m \approx \left(\frac{S_1 \cos \theta_1 - S_2 \cos \theta_2}{m_1^2 - m_2^2} \right)^2 \approx \left(\frac{m_1^2 + m_2^2}{m_1^2 - m_2^2} \right)^2. \quad (5.2)$$

Thus we see that for large mass ratios, the spin locking does not occur until very late in the inspiral, while for equal mass systems it is important even for a relatively wide separation. This result is consistent with the recent findings by Buonanno et al. [7] that find the best fitting factors in the cases of nearly equal masses, further emphasizing the similarity between their effective spin method and the equilibrium solutions of this paper.

The dependence of spin locking on the mass ratio is shown in Figure 9 for maximally spinning black holes with $\theta_1(t_0) = 10^\circ$. For $m_1 : m_2 = 0.55 : 0.45$, the spin locking is very strong at the end of the inspiral ($r/m = 10$), as we saw in Figure 5. With increasing mass ratios of $m_1 : m_2 = 3 : 2$, $3 : 1$, and $9 : 1$, the resonance behavior grows increasingly weaker, showing a smaller influence on the initially uniform distribution of $(\theta_{12}, \Delta\phi)$. However, it should be noted that since the inspiral time scales as μ^{-1} , the higher mass ratio binaries also spend a longer time at smaller separations, producing many more cycles in the waveform at late times. Thus the equilibrium solutions may still give good estimates for waveform templates even for the moderate mass ratios that would be expected for NS-BH binaries.

VI. EFFECTS OF ECCENTRICITY AND SPIN MAGNITUDE

For the sake of simplicity, most of the computations carried out so far have had circular orbits throughout the inspiral. However, it is relatively straightforward to include a non-zero eccentricity and evolve it along with the other system variables according to equations (2.14, 2.15, 2.16). As shown in Peters [23], a high eccentricity has the effect of speeding up the inspiral time scale. Yet as we see from equations (2.10a, 2.10b), eccentricity also increases the precession rate, accelerating the rate of spin evolution.

For the nearly equal mass cases discussed in Section IV, we find that including a high initial eccentricity ($a_0 = 2000m, e_0 = 0.9$) reduces the overall effect of the spin locking, but only slightly. A sinusoidal plot of $(\theta_{12}, \Delta\phi)$ analogous to Figure 5 shows the same qualitative behavior for eccentric orbits, with marginally more scatter in the final distribution. This suggests that the increase in the inspiral rate slightly prevails over the increased precession rate and the spins do not have as much time to get locked into their equilibrium states.

While we have not yet discovered a BH-BH binary, the known NS-NS systems show a range of eccentricities up to $e \approx 0.6$, presumably due to the variation of initial kick velocities [16]. By integrating (2.14) and (2.15), it is clear that all these known systems will circularize long before the spin locking becomes important, and certainly before entering the detector band [11].

There is also the possibility of forming high eccentricity BH-BH binaries through many-body exchange interactions in the cores of dense globular clusters, which are then ejected and merge within a Hubble time [14]. Yet even for these systems, the merger time scale is long enough that the circular orbit approximation is most likely a reasonable one. In the case of the high mass ratios described in Section V, high eccentricities are much more likely. However, as was mentioned above, in such a system the contribution of the smaller spin is negligible and the solar mass black hole can be treated accurately as a point mass. Furthermore, from (5.2) we see that spin effects are important at a much later stage for high mass ratios, giving more time for the system to circularize, again justifying the circular orbit approximation.

We have also investigated the effects of non-maximal spin parameters on the evolution of the spin distributions. While equation (5.1) suggests that the resonant locking effects might fall off for smaller values of S_1 and S_2 , in practice we find a relatively weak dependence on the magnitude of the spin parameter for $a/m = S/m^2 > 0.5$. Figure 10 shows the probability distributions of $(\theta_{12}, \Delta\phi)$ near the end of inspiral for a variety of spin magnitudes. Each system has the same mass ratio $m_1 : m_2 = 11 : 9$ and initial spin-orbit angle $\theta_1(t_0) = 10^\circ$. Even for spins as small as $a/m = 0.25$ we see significant spin locking at the end of inspiral. Interestingly, the final distribution for $a/m = 0.5$ and $m_1 : m_2 = 11 : 9$ is almost identical to that of $a/m = 1$ and $m_1 : m_2 = 3 : 1$ (cf. Figs. 9 and 10), perhaps pointing to another relation in the evolution equations that could be used to reduce further the dimensionality of the total search space, analogous to the effective spins described in [7].

VII. CONCLUSIONS

We have derived a set of orbit-averaged post-Newtonian equations of motion for two spinning point masses throughout the binary inspiral. This makes it possible to model the evolution of the relative spin orientations over a large range of time scales. One important result is the discovery of nontrivial equilibrium solutions that allow the system to remain locked in a given orientation, exhibiting stable resonance behavior. Through the loss of energy and angular momentum to gravitational radiation, a binary system can undergo a transition from an unlocked to locked position, in turn significantly affecting the distribution function of the spins in parameter space.

This behavior appears to be due in large part to the constraints placed on the orbital angular momentum and spin vectors within the precession framework. Conservation of total angular momentum $\mathbf{J} = \mathbf{L} + \mathbf{S}$ restrict the available regions of parameter space accessible to the system over short time scales. In this context, it may be more helpful to think of the spin interactions as “spin-orbit-spin” coupling. The precession of \mathbf{S}_1 will change the orientation of \mathbf{L} , which in turn affects the precession of \mathbf{S}_2 . In an effort to better understand the origin of this behavior, we have repeated many of the evolution calculations, now with the direct spin-spin precession terms (order 1.5PN) turned off. This can be done trivially by removing the terms proportional to spin in equations (2.10a, 2.10b). Interestingly, the effect is almost negligible, giving qualitatively the same results shown in Figures 5 and 6. However, we should be careful to note that this is not quite the same condition as applied in [3, 6], where the analysis is limited to spin-orbit interactions simply by disregarding the spin of the smaller body. The approach here is more closely analogous to the effective spin method of Buonanno et al. [7]. We believe their high level of success in using a single pseudo-physical spin may be closely related to the resonances described in this paper.

Coupled with an estimate for the initial spin-orbit orientation from binary evolution codes, the analysis presented in this paper can be used to predict the distribution of spins relevant for gravitational wave detectors and waveform templates. By limiting the template library to the family of equilibrium solutions, we could greatly reduce the size of the parameter search space, in turn increasing the chances of signal detection. The spin orientation at small orbital separations, shortly before merger, could also be very useful information for studying the highly relativistic plunge regime, where the post-Newtonian approximation breaks down. Among other difficulties, the problem of black holes merging in numerical relativity is plagued by a lack of insight into the appropriate initial conditions. The results of this paper may serve to provide some of that insight.

Directions for future work include modeling a vastly expanded parameter space and in turn studying the resonance behavior over a greater region of astrophysical interest. These studies should include both LIGO and LISA type sources, as well as continuing to investigate other evidence for spin-orbit and spin-spin interactions, such as the electromagnetic signatures of supermassive black hole mergers and binary pulsar systems. Similarly, comprehensive calculations of compact binary formation scenarios are needed to provide reasonable initial data for the inspiral evolution.

As we have mentioned repeatedly throughout this paper, a major part of the detection strategy for gravitational wave observatories is that of template matching. We propose using the equilibrium solutions as a subset of the parameter space as a way to maximize the computational efficiency of matched filtering. A next step would be to quantify this presumption by calculating the fitting factors of waveforms from off-resonance and near-resonance systems compared to those of the exact equilibrium solutions, similar to the analysis of [7]. This approach would also provide concrete

predictions for detection rates as a function of the source distributions and could be used to give stronger upper limits on binary coalescence rates. By using this set of physical templates, the intrinsic binary parameters of the compact system should be determined with greater precision than attainable by using a pseudo-physical template family.

Aside from the potentially large impact on gravitational wave detection, the spin locking result is also of considerable interest for general dynamical systems exhibiting resonance behavior. We have made some progress in understanding the geometry of this resonance and how systems can be captured into it via radiation reaction. A more comprehensive study of the dynamics, including the possible identification of other resonances not yet discovered, could in turn predict new signatures to look for in gravitational wave signals. Of particular interest would be the possibility of finding overlapping resonance regions, classically an important breeding ground for chaotic systems [25]. One promising approach to the resonance problem is the use of conservative Hamiltonian equations of motion (e. g. [26, 27, 28]), as opposed to the Lagrangian methods used here and in most other post-Newtonian calculations. The Hamiltonian approach more closely resembles the classical formulations of dynamic systems like the Solar System and coupled oscillators that show many examples of resonance behavior [24], and thus could give us greater insight into the dynamics of compact binaries.

VIII. ACKNOWLEDGMENTS

I would like to thank Alessandra Buonanno, Scott Hughes, and Vicky Kalogera for their very detailed and helpful comments. Many thanks to Edmund Bertschinger for his continued support and encouragement. This work was supported in part by NASA grant NAG5-13306.

APPENDIX A: DERIVATION OF THE EVOLUTION EQUATIONS

Assuming elliptical orbits with semimajor axis a and eccentricity e , we define a coordinate system with the origin at the occupied focus, $\hat{\mathbf{e}}_z = \mathbf{L}_N/|\mathbf{L}_N|$, and $\hat{\mathbf{e}}_x$ aligned with the ellipse's pericenter. Then \mathbf{r} is given by

$$\mathbf{r} = [r \cos f, r \sin f, 0], \quad (\text{A1})$$

where f is the true anomaly. From the standard binary relations for elliptical orbits, we define the specific angular momentum of the reduced two-body system as

$$l \equiv r^2 \dot{f} = \sqrt{ma(1-e^2)}, \quad (\text{A2})$$

with

$$r = \frac{a(1-e^2)}{1+e \cos f} \quad (\text{A3})$$

and the total mass $m = m_1 + m_2$. We can then change variables from $dt \rightarrow df$ to get

$$dt = \frac{[a(1-e^2)]^{3/2}}{m^{1/2}(1+e \cos f)^2} df. \quad (\text{A4})$$

Averaging the \mathbf{r} -dependent part of equations (2.2a, 2.2b) over one binary period P gives

$$\begin{aligned} \frac{1}{P} \int_0^P \frac{dt}{r^3} (\hat{\mathbf{r}} \cdot \mathbf{S}) \hat{\mathbf{r}} &= \frac{1}{2\pi a^{3/2}} \int_0^{2\pi} \frac{df (1+e \cos f)}{[a(1-e^2)]^{3/2}} (S^x \cos f + S^y \sin f) (\cos f \hat{\mathbf{e}}_x + \sin f \hat{\mathbf{e}}_y) \\ &= \frac{\mathbf{S} - (\hat{\mathbf{e}}_z \cdot \mathbf{S}) \hat{\mathbf{e}}_z}{2a^3(1-e^2)^{3/2}}. \end{aligned} \quad (\text{A5})$$

Then the orbit-averaged precession vectors are

$$\bar{\mathbf{\Omega}}_1 = \frac{1}{P} \int_0^P dt \mathbf{\Omega}_1 = \frac{1}{a^3(1-e^2)^{3/2}} \left[\left(2 + \frac{3m_2}{2m_1} - \frac{3\mathbf{S}_2 \cdot \mathbf{L}_N}{L_N^2} \right) \mathbf{L}_N + \frac{1}{2} \mathbf{S}_2 \right] \quad (\text{A6})$$

and

$$\bar{\mathbf{\Omega}}_2 = \frac{1}{P} \int_0^P dt \mathbf{\Omega}_2 = \frac{1}{a^3(1-e^2)^{3/2}} \left[\left(2 + \frac{3m_1}{2m_2} - \frac{3\mathbf{S}_1 \cdot \mathbf{L}_N}{L_N^2} \right) \mathbf{L}_N + \frac{1}{2} \mathbf{S}_1 \right]. \quad (\text{A7})$$

As explained in the text, we are primarily interested in the *relative* orientation of the three vectors \mathbf{L}_N , \mathbf{S}_1 , and \mathbf{S}_2 , a problem that can be reduced to only four variables ($L, \theta_1, \theta_2, \Delta\phi$) in the case of circular orbits. To avoid certain sign ambiguities, it is actually more convenient to use five variables, defined as following (normalizing to $m = 1$):

$$L \equiv |\mathbf{L}_N| = \mu r^{1/2}, \quad (\text{A8a})$$

$$z_1 \equiv \cos \theta_1 = \frac{\mathbf{S}_1 \cdot \mathbf{L}_N}{S_1 L}, \quad (\text{A8b})$$

$$z_2 \equiv \cos \theta_2 = \frac{\mathbf{S}_2 \cdot \mathbf{L}_N}{S_2 L}, \quad (\text{A8c})$$

$$\beta \equiv \cos \theta_{12} = \frac{\mathbf{S}_1 \cdot \mathbf{S}_2}{S_1 S_2}, \quad (\text{A8d})$$

$$\alpha \equiv \frac{\mathbf{L}_N \cdot (\mathbf{S}_1 \times \mathbf{S}_2)}{L S_1 S_2}. \quad (\text{A8e})$$

Under radiation reaction, the separation r will monotonically decrease throughout the evolution, allowing us to define a new time variable $\tau \equiv r_0 - r$ so that, from (2.5),

$$\frac{d}{dt} = \frac{64\mu}{5r^3} \frac{d}{d\tau}. \quad (\text{A9})$$

In these coordinates, with an over-dot representing $d/d\tau$, the equations of motion are:

$$\dot{L} = -\frac{\mu^2}{2L}, \quad (\text{A10a})$$

$$\dot{z}_1 = \frac{15}{128\mu} \alpha S_2 \left(\frac{1}{m_2} - \frac{S_1 z_1}{L} \right), \quad (\text{A10b})$$

$$\dot{z}_2 = \frac{15}{128\mu} \alpha S_1 \left(\frac{S_2 z_2}{L} - \frac{1}{m_1} \right), \quad (\text{A10c})$$

$$\dot{\beta} = \frac{15}{128\mu} \alpha L \left(\frac{m_2}{m_1} - \frac{m_1}{m_2} + \frac{S_1 z_1 - S_2 z_2}{L} \right), \quad (\text{A10d})$$

$$\dot{\alpha} = \frac{1}{\alpha} \left[z_1 z_2 \dot{\beta} + \beta (z_1 \dot{z}_2 + z_2 \dot{z}_1) - z_1 \dot{z}_1 - z_2 \dot{z}_2 - \beta \dot{\beta} \right]. \quad (\text{A10e})$$

From these functions, the original variable $\Delta\phi$ can be easily restored through

$$\Delta\phi = \tan^{-1}[\alpha, (\beta - z_1 z_2)]. \quad (\text{A11})$$

For reference, equations (A10b-d) can be compared with similar results derived in [9], equations (2a-c) and [7], equations (17-19).

-
- [1] T. A. Apostolatos, Phys. Rev. D **52**, 605 (1995).
 - [2] P. Grandclement, V. Kalogera, and A. Vecchio, Phys. Rev. D **67**, 042003 (2003).
 - [3] A. Buonanno, Y. Chen, and M. Vallisneri, Phys. Rev. D **67**, 104025 (2003).
 - [4] P. Grandclement and V. Kalogera, Phys. Rev. D **67**, 082002 (2003).
 - [5] P. Grandclement, M. Ihm, V. Kalogera, and K. Belczynski, Phys. Rev. D **69**, 102002 (2004).
 - [6] Y. Pan et al., Phys. Rev. D **69**, 104017 (2004).
 - [7] A. Buonanno, Y. Chen, Y. Pan, and M. Vallisneri, Phys. Rev. D, submitted (2004). [gr-qc/0405090]
 - [8] T. A. Apostolatos, C. Cutler, G. J. Sussman, and K. S. Thorne, Phys. Rev. D **49**, 627 (1994).
 - [9] T. A. Apostolatos, Phys. Rev. D **54**, 2438 (1996).
 - [10] V. Kalogera, ApJ **541**, 319 (2000).
 - [11] K. Belczynski, V. Kalogera, and T. Bulik, ApJ **572**, 407 (2002).
 - [12] E. Pfahl et al., ApJ **574**, 364 (2002).
 - [13] P. Nutzman et al., ApJ accepted (2004). [astro-ph/0402091]
 - [14] S. F. Portegies-Zwart and S. L. W. McMillan, ApJ **528**, L17 (2000).
 - [15] A. G. Lyne et al., Science **303**, 1153 (2004).
 - [16] B. Willens and V. Kalogera, ApJ **603**, L101 (2004).
 - [17] D. Merritt and R. D. Ekers, Science **297**, 1310 (2002).
 - [18] S. A. Hughes and R. D. Blandford, ApJ **585**, L101 (2003).
 - [19] L. E. Kidder, Phys. Rev. D **52**, 821 (1995).
 - [20] J. Baker, M. Campanelli, and C. O. Lousto, Phys. Rev. D **65**, 044001 (2002).
 - [21] M. Favata, S. A. Hughes, and D. E. Holz, ApJ **607**, L5 (2004).
 - [22] L. E. Kidder, C. M. Will, and A. G. Wiseman, Phys. Rev. D **47**, 4183 (1993).
 - [23] P. C. Peters, Phys. Rev. **136**, B1224 (1964).
 - [24] C. D. Murray and S. F. Dermott, *Solar System Dynamics* (Cambridge University Press, Cambridge, 1999).
 - [25] G. J. Sussman and J. Wisdom, *Structure and Interpretation of Classical Mechanics* (MIT Press, Cambridge MA, 2001).
 - [26] T. Damour and G. Schafer, Nuovo Cimento Soc. Ital. Fis. B **101**, 127 (1988).
 - [27] P. Jaranowski and G. Schafer, Phys. Rev. D **57**, 7274 (1998).
 - [28] T. Damour, Phys. Rev. D **64**, 124013 (2001).
 - [29] J. D. Schnittman and F. A. Rasio, Phys. Rev. Lett. **87**, 121101 (2001).
 - [30] N. J. Cornish and J. Levin, Class. and Quant. Grav. **20**, 1649 (2003).
 - [31] C. L. Fryer, ApJ **522**, 413 (1999).
 - [32] Yu. Levin and A. M. Beloborodov, ApJ **509**, L33 (2003).

FIG. 1: Schematic diagram of the spin and orbital angular momentum vectors. The coordinate system is defined such that \mathbf{L}_N is along the z -axis and (θ_1, θ_2) are the respective angles between \mathbf{L}_N and $(\mathbf{S}_1, \mathbf{S}_2)$. The projection of \mathbf{S}_1 onto the x - y plane is defined to be along the x -axis so the azimuthal spin angles are $\phi_1 = 0$ and $\phi_2 = \Delta\phi$.

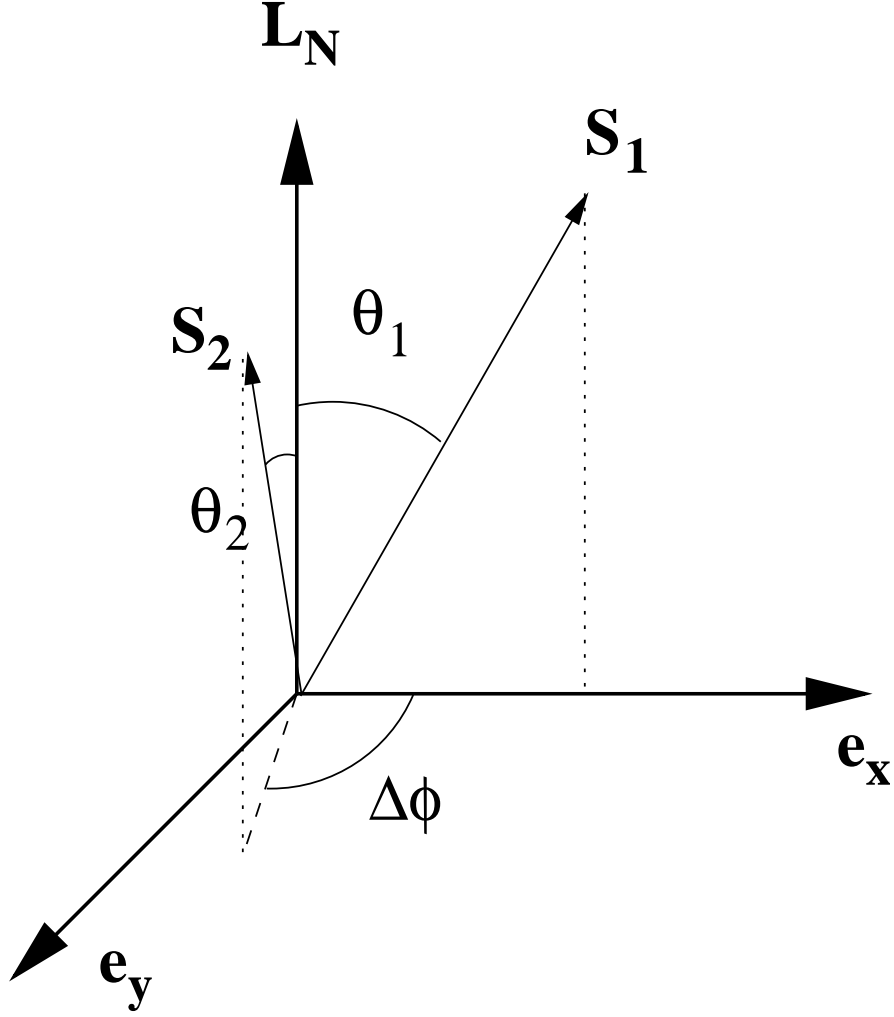


FIG. 2: Equilibrium solutions of equation (3.5) for the case of maximally spinning black holes with normalized masses ($m_1 = 0.55, m_2 = 0.45$) and spin alignment $\Delta\phi = 0^\circ$. The solution curves are labeled by their different values of the orbital angular momentum L_N , so that equilibrium systems evolving under radiation reaction move along subsequent curves with decreasing L_N (corresponding to $r/m \approx 260, 150, 65, 16, 4$). The labels 'A' and 'B' refer to the initial conditions for Figures 4a and 4b, both with $L_N(t_0) = 4$.

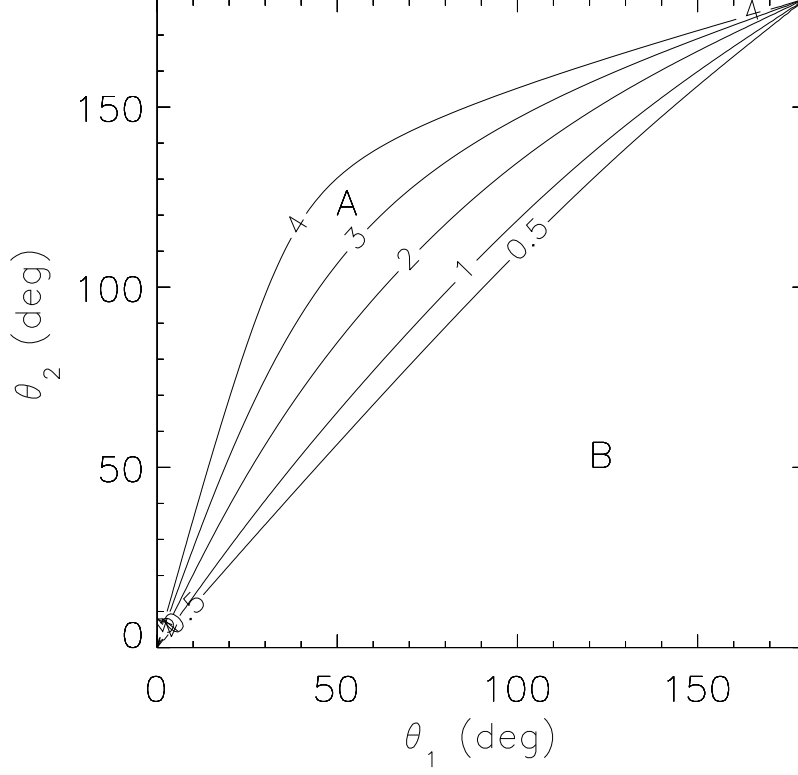


FIG. 3: Equilibrium solutions of equation (3.5) for the case of maximally spinning black holes with normalized masses ($m_1 = 0.55, m_2 = 0.45$) and spin anti-alignment $\Delta\phi = 180^\circ$. The solution curves are labeled by their different values of the orbital angular momentum L_N , so that equilibrium systems evolving under radiation reaction move along subsequent curves with decreasing L_N (corresponding to $r/m \approx 260, 150, 65, 16, 4$). Solid curves correspond to stable equilibrium orientations, while the dashed curves are the quasi-stable solutions described in the text. The label 'C' refers to the unstable initial conditions of Figure 4c, with $L_N(t_0) = 1$.

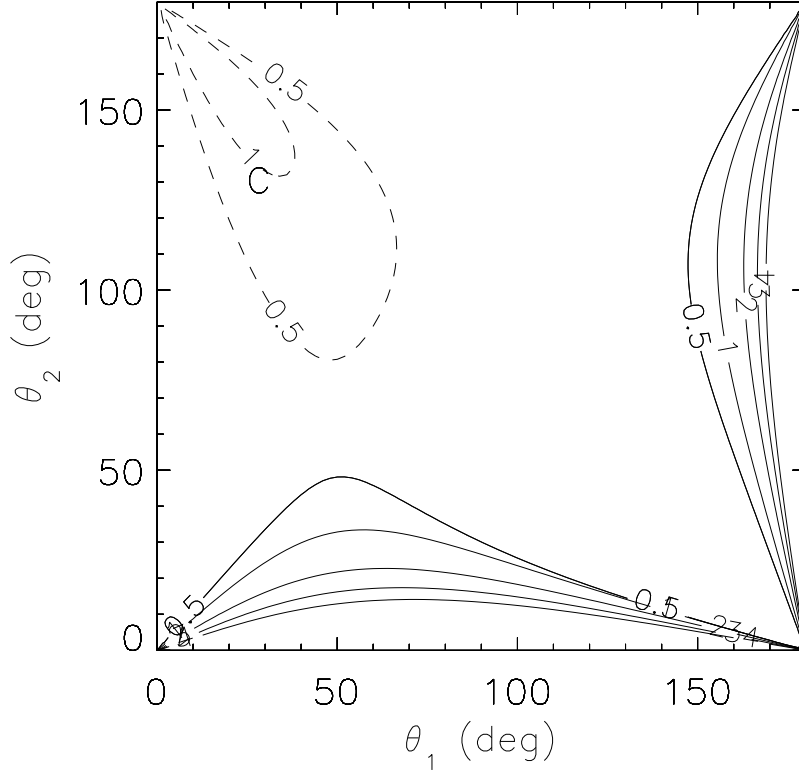


FIG. 4: Integrated phase difference $[\Delta\phi(t)]_{\text{tot}}$ between two precessing spin vectors. Examples are shown for initial conditions (a) near a stable equilibrium with $\theta_1 = 50^\circ, \theta_2 = 120^\circ, \Delta\phi = 0^\circ$, and $L_N = 4$; (b) far away from equilibrium with $\theta_1 = 120^\circ, \theta_2 = 50^\circ, \Delta\phi = 0^\circ$, and $L_N = 4$; (c) near a quasi-stable equilibrium with $\theta_1 = 30^\circ, \theta_2 = 133^\circ, \Delta\phi = 180^\circ$, and $L_N = 1$ (compare with Figures 2 and 3). For all three cases, radiation reaction has been turned off.

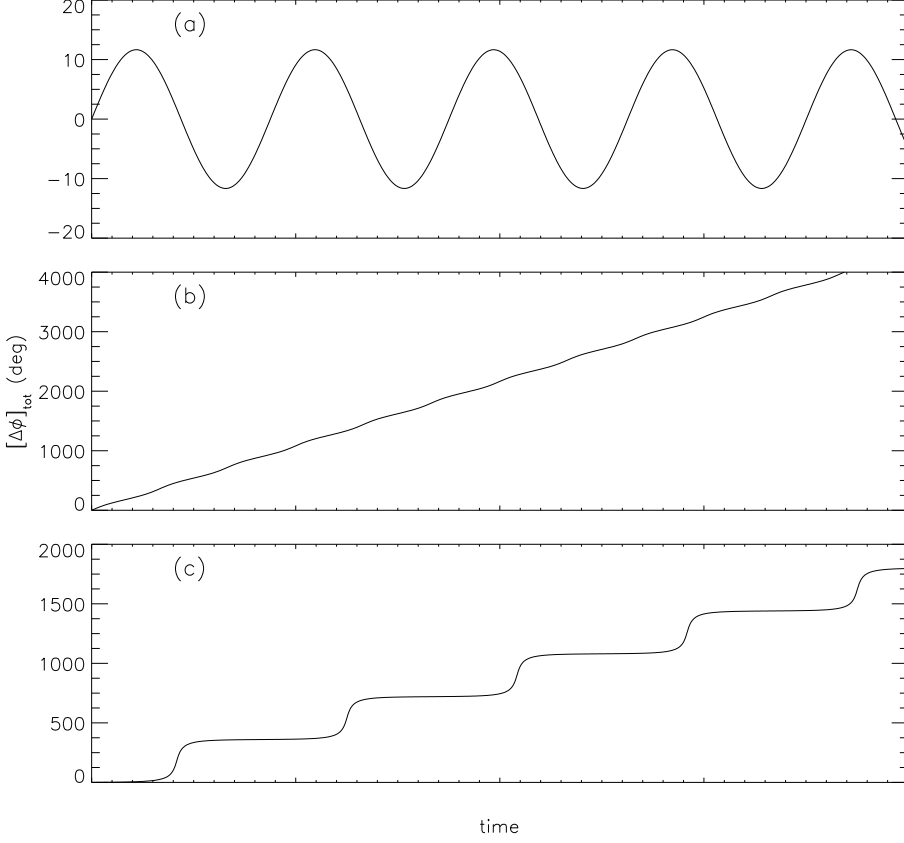


FIG. 5: Sinusoidal projections of spin parameter space $[\theta_{12} \equiv \cos^{-1}(\hat{\mathbf{S}}_1 \cdot \hat{\mathbf{S}}_2), \Delta\phi]$. A sinusoidal projection maps spherical coordinates (θ, ϕ) to flat Cartesian coordinates $(\phi \sin \theta, \theta)$ with equal solid angles mapping to equal areas. The snapshots show a random sample of initial conditions with $r(t_0) = 1000m$ evolving under radiation reaction at times when $r/m = 1000, 250, 125, 10$. The masses of the two compact objects are similar, with $m_1 = 0.55$ and $m_2 = 0.45$, and both have maximal spins. The initial spin of the larger mass is closely aligned with the orbital angular momentum: $\theta_1(t_0) = 10^\circ$.

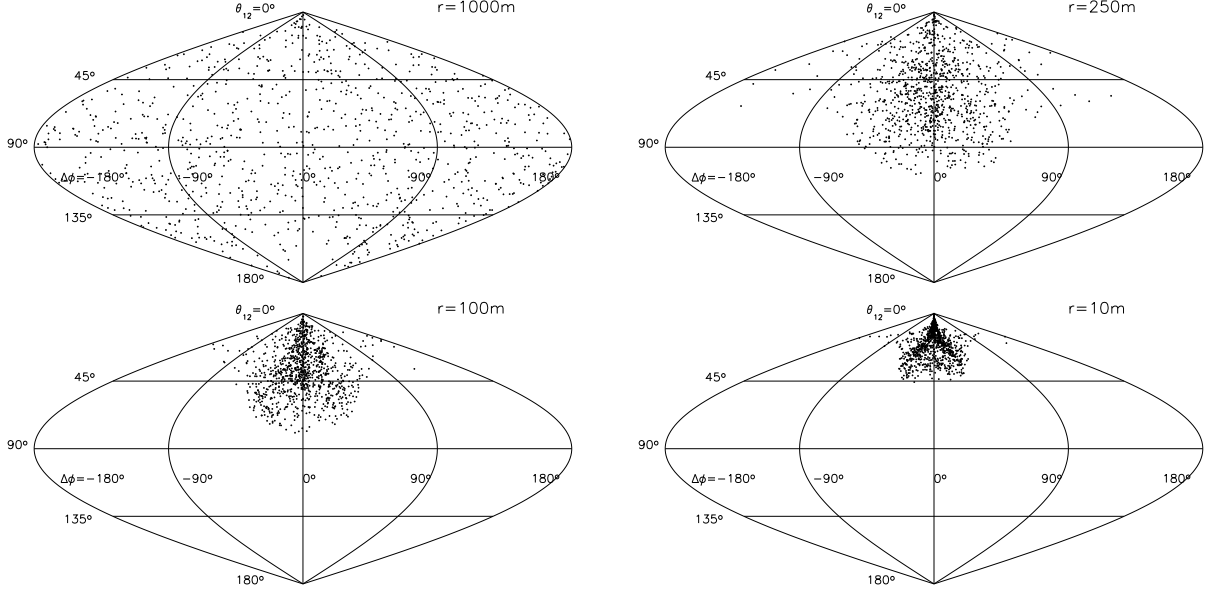


FIG. 6: Sinusoidal projections of spin parameter space $[\theta_{12} \equiv \cos^{-1}(\hat{\mathbf{S}}_1 \cdot \hat{\mathbf{S}}_2), \Delta\phi]$, as in Figure 5. The snapshots show a random sample of initial conditions with $r(t_0) = 1000m$ evolving under radiation reaction at times when $r/m = 1000, 250, 125, 10$. The masses of the two compact objects are similar, with $m_1 = 0.55$ and $m_2 = 0.45$, and both have maximal spins. The initial spin of the larger mass is misaligned with the orbital angular momentum: $\theta_1(t_0) = 170^\circ$.

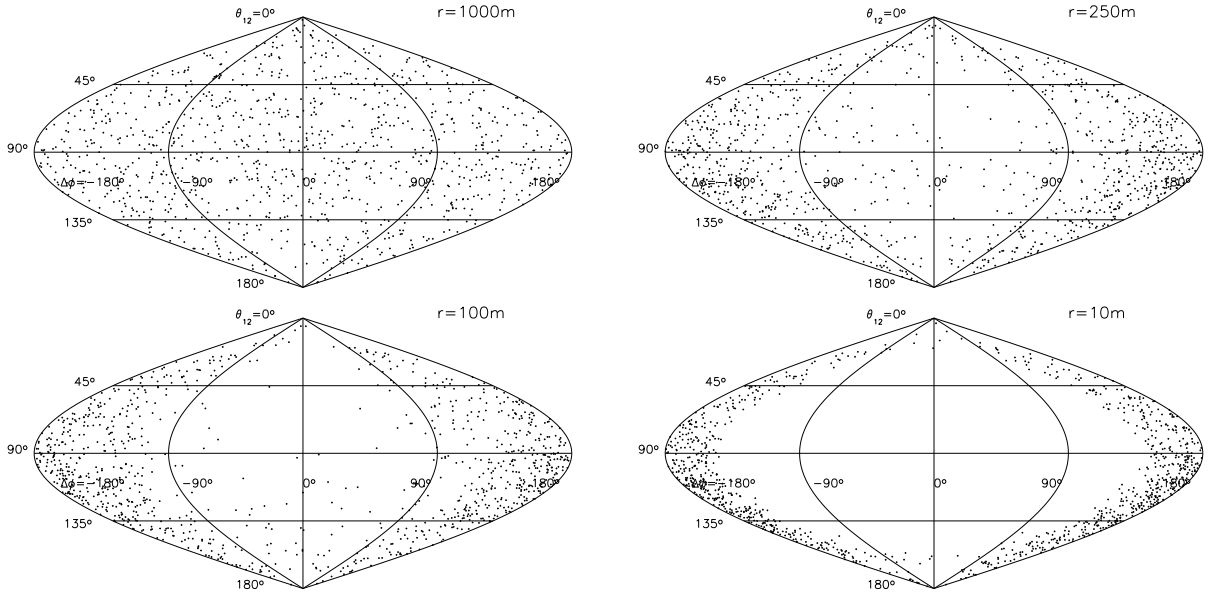


FIG. 7: Probability distribution for spin orientations (a) $\cos\theta_{12}$ and (b) $\Delta\phi$ near the end of inspiral ($r/m = 10$). The distributions are plotted for different values of $\theta_1(t_0)$ with $r(0) = 1000m$ in all cases. Both black holes are maximally spinning with similar masses $m_1 = 0.55, m_2 = 0.45$. When the larger spin is initially aligned with the orbital angular momentum ($\theta_1 < 90^\circ$), the final spins tend to align ($\Delta\phi \rightarrow 0^\circ, \cos\theta_{12} \rightarrow 1$).

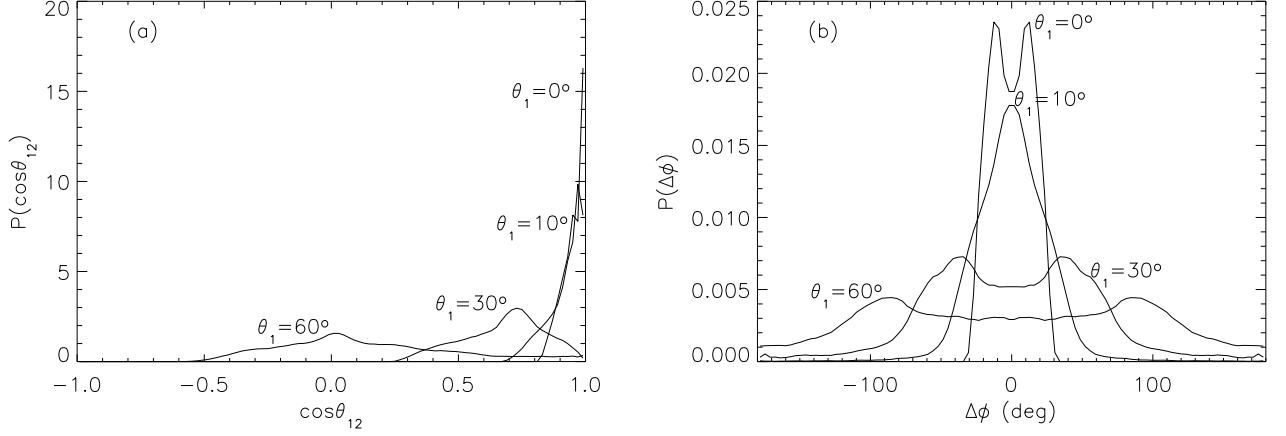


FIG. 8: Probability distribution for spin orientations (a) $\cos\theta_{12}$ and (b) $\Delta\phi$ near the end of inspiral. All parameters are as in Figure 7, yet with the larger spin initially misaligned with the orbital angular momentum [$\theta_1(t_0) > 90^\circ$]. In these cases, the final spins also tend to be anti-aligned with each other ($\Delta\phi \rightarrow \pm 180^\circ, \cos\theta_{12} \rightarrow -1$), although $\cos\theta_{12}$ is less sensitive to the initial conditions, as can be seen from Figure 6.

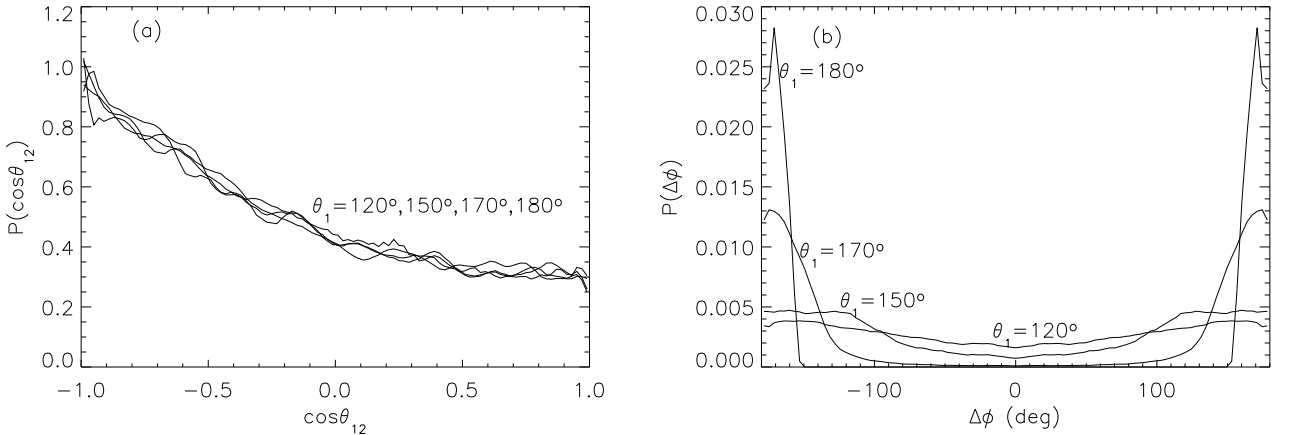


FIG. 9: Probability distribution for spin orientations (a) $\cos\theta_{12}$ and (b) $\Delta\phi$ near the end of inspiral. The initial spin orientation has $\theta_1 = 10^\circ$ and uniform distribution of θ_2 . Each system has maximal spins but a different mass ratio $m_1 : m_2$. The spin-locking resonance is clearly more important for nearly equal mass systems, as seen from equation (5.2).

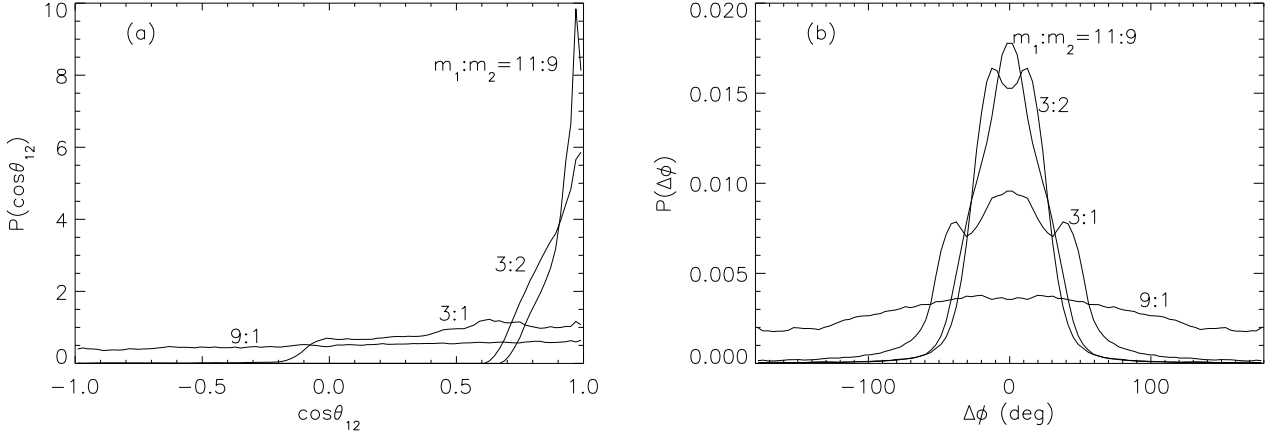


FIG. 10: Probability distribution for spin orientations (a) $\cos\theta_{12}$ and (b) $\Delta\phi$ near the end of inspiral. The initial spin orientation has $\theta_1 = 10^\circ$ and uniform distribution of θ_2 . Each system has $m_1 = 0.55, m_2 = 0.45$ but different values for the black hole spin parameter a/m . The evolution is largely independent of the spin magnitude for moderately values of $a/m > 0.5$, while even systems with small spin parameters exhibit significant spin locking.

